Paper:
Yusenko, K., Bykova, E., Bykov, M., Riva, S., Crichton, W., Yusenko, M., Sukhikh, A., Arnaboldi, S., Hanfland, M., et. al. (2017). Ir–Re binary alloys under extreme conditions and their electrocatalytic activity in methanol oxidation. *Acta Materialia, 139*, 236-243.
http://dx.doi.org/10.1016/j.actamat.2017.08.012

Accepted Manuscript

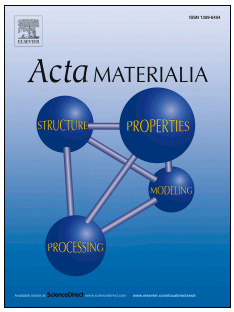

IrRe binary alloys under extreme conditions and their electrocatalytic activity in methanol oxidation

Kirill V. Yusenko, Elena Bykova, Maxim Bykov, Sephira Riva, Wilson A. Crichton, Maria V. Yusenko, Aleksandr S. Sukhikh, Serena Arnaboldi, Michael Hanfland, Leonid S. Dubrovinsky, Sergey A. Gromilov

PII: S1359-6454(17)30655-9

DOI: 10.1016/j.actamat.2017.08.012

Reference: AM 13973

To appear in: *Acta Materialia*

Received Date: 24 March 2017

Revised Date: 30 June 2017

Accepted Date: 7 August 2017

Please cite this article as: K.V. Yusenko, E. Bykova, M. Bykov, S. Riva, W.A. Crichton, M.V. Yusenko, A.S. Sukhikh, S. Arnaboldi, M. Hanfland, L.S. Dubrovinsky, S.A. Gromilov, IrRe binary alloys under extreme conditions and their electrocatalytic activity in methanol oxidation, *Acta Materialia* (2017), doi: 10.1016/j.actamat.2017.08.012.

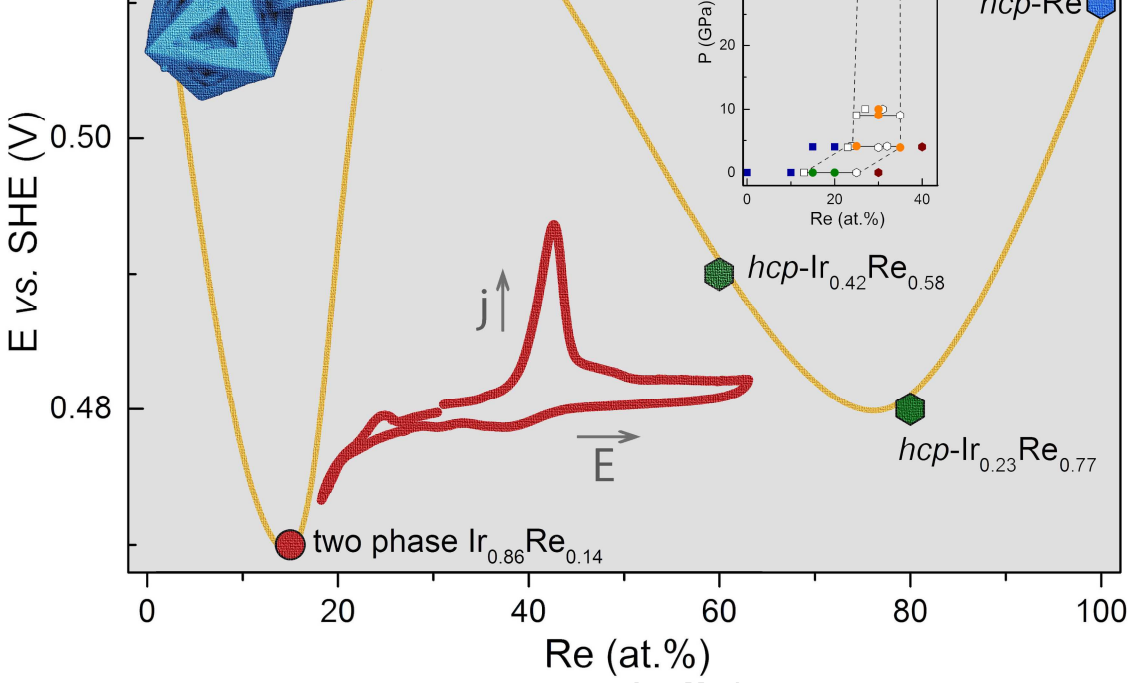
E vs. SHE (V)
0.50
0.48
0
20
40
60
80
100
Re (at.%)
P (GPa)
0
10
20
0
20
40
Re (at.%)
hcp-Re
hcp-Ir0.42Re0.58
hcp-Ir0.23Re0.77
two phase Ir0.86Re0.14
j
E

Kirill V. Yusenko,[a,b,*] Elena Bykova,[c] Maxim Bykov,[d] Sephira Riva,[a]

Wilson A. Crichton,[e] Maria V. Yusenko,[f] Aleksandr S. Sukhikh,[g,h] Serena Arnaboldi,[i]

Michael Hanfland,[e] Leonid S. Dubrovinsky,[d] Sergey A. Gromilov[f,g]

[a]College of Engineering, Swansea University, Bay Campus, SA1 8EN, Wales, UK

[b]Institute of Solid State Chemistry, Pervomaiskaia str. 91, 620990 Ekaterinburg, Russia

[c]Photon Sciences, Deutsches Elektronen-Synchrotron, Notkestrasse 85, D-22603 Hamburg, Germany

[d]Bayerisches Geoinstitut, Universität Bayreuth, D-95440 Bayreuth, Germany

[e]Königsberger Str. 136, D-48157, Münster, Germany

[f]ESRF-The European Synchrotron, 71 avenue des Martyrs, 38000, Grenoble, France

[g]Department of Naturel Science, Novosibirsk State University, Pirogova str. 2, 630090 Novosibirsk, Russia

[h]Department of Crystal Chemistry, Nikolaev Institute of Inorganic Chemistry, Lavrentiev ave. 3, 630090 Novosibirsk, Russia

[i]Dipartimento di Chimica, Università degli Studi di Milano, 20133 Milano, Italy

* Corresponding author: College of Engineering, Swansea University, Bay Campus, SA1 8EN, Wales, UK; e-mail: k.yusenko@swansea.ac.uk

Abstract. The formation of the *hcp*-$Ir_{0.70}Re_{0.30}$ alloy from the single-source precursor $(NH_4)_2[Ir_{0.70}Re_{0.30}Cl_6]$ upon heating in hydrogen atmosphere can be associated with the formation of two intermediates: a crystalline iridium-based intermediate and an *fcc*-structured alloy. Ir—Re alloys show lower thermal expansion coefficients and smaller

phase diagram. The miscibility gap between *hcp* and *fcc* alloys slightly shifts towards the rhenium side below 4 GPa. Above 4 GPa, the miscibility gap does not drift with pressure and narrows with compression. The electrocatalytic activity of Ir—Re alloys has been tested for methanol oxidation in acidic water solution. Ir—Re alloys show higher electrocatalytic activity in comparison with pure Ir and Re, which makes them perspective candidates for fuel cells application. The highest electrocatalytic activity has been obtained for the two-phase $Ir_{0.85}Re_{0.15}$ composition.

Keywords: high-pressure, high-temperature, alloys, phase diagrams, X-ray diffraction, electrocatalysis

1. Introduction

The detailed investigation of binary alloys and their phase diagrams provides the basement for further progress in the development of multicomponent alloy compositions. Pure metals and binary alloys can be considered important models for further progression towards more complex systems, such as high-entropy alloys, metallic glasses, metallic foams and heterogeneous metal matrix composites. Refractory alloys based on platinum group metals play an important role as materials with outstanding mechanical, thermal and chemical stability. Nevertheless, due to their high melting points and price their applications are still limited and information about their properties is fragmented.

Alloys based on platinum group metals with rhenium, especially Pt—Re alloys, were extensively investigated due to their extraordinary thermal stability and catalytic properties. At the same time, Ir—Re and Rh—Re alloys were investigated sporadically

were applied to the construction of rocket combustion chambers [9].

Pure platinum group metals were broadly investigated under extreme conditions. Nevertheless, their alloys have seldom been studied. Only Ir—Os alloys were tested under high-pressure high-temperature conditions *in situ* up to 140 GPa and 3000°C [10-11], and the Ir—Re system has been investigated under high-temperature high-pressure up to 9 GPa and 2000°C *ex situ* using a belt press [12-16]. High-temperature high-pressure studies may lead to a deeper understanding of the stability of ultra-hard ultra-incompressible alloys upon extreme conditions and eventually be exploited as tools for the construction of realistic pressure-dependent phase diagrams. These are especially needed to predict alloys properties under working conditions as well as to understand the formation of their metallic minerals from the melt in the Earth Core.

The Ir—Re binary metallic system has been investigated in detail during the last decade. Recently, existing experimental data have been critically reviewed with the aim of creating a realistic model for the Ir—Re ambient pressure binary phase diagram [2]. According to experimental data, the peritectic binary Ir—Re phase diagram has a miscibility gap between *fcc*- and *hcp*-structured alloys at 20 and 30 at.% Re. The Ir—Re phase diagram has been calculated using a sub-regular solution model based on experimental crystallographic and thermodynamic data (Fig. 1) [2].

Several Ir—Re alloys were prepared by arc-melting, high-temperature annealing and thermal decomposition of single-source precursors. Existing experimental data for single-phase Ir—Re alloys are summarized in the supplementary table S1. Atomic

$$V/Z_{hcp} = 14.14(6) + 0.14(2)\cdot x_{Re} + 0.43(5)\cdot x_{Re}^2 \qquad (1),$$

$$V/Z_{fcc} = 14.15(1) + 0.17(1)\cdot x_{Re} + 0.82(7)\cdot x_{Re}^2 \qquad (2),$$

where atomic volumes, V/Z (V is a volume of the elemental cell and Z corresponds to the number of atoms in the elemental cell, with $Z = 2$ for *hcp* and $Z = 4$ for *fcc* alloys) are plotted *versus* atomic rhenium composition, x_{Re} (Fig. 1). *Hcp* and *fcc* alloys follow two functions, both displaying small negative deflection from linearity (<2 %). The describing functions herein described can be used to estimate the composition of Ir—Re solid solutions with known lattice parameters.

In the present study, we report the investigation of *hcp*-structured Ir—Re alloys under high-temperature high-pressure conditions. Our primary goal is the construction of a pressure-dependent binary phase diagram for a system constituted by incompressible metals with ultra-high melting points. The compressibility curve for *hcp*-$Ir_{0.70}Re_{0.30}$ was collected using *in situ* X-ray powder diffraction in diamond anvil cells and a large-volume press. To investigate the formation of *hcp*-$Ir_{0.70}Re_{0.30}$ from the single-source bimetallic precursor $(NH_4)_2[Ir_{0.70}Re_{0.30}Cl_6]$ upon heating in hydrogen atmosphere, we emplyed *in situ* powder X-ray diffraction. Finally, we performed preliminary tests of the electrocatalytic activity of *hcp*-structured Ir—Re alloys for methanol oxidation in acidic solution, as model systems for fuel cells.

2. Experimental details

Ir_xRe_{1-x} alloys were prepared using single-source bimetallic precursors $(NH_4)_2[Ir_xRe_{1-x}Cl_6]$ (x = 0.23, 0.42, 0.70, 0.71, 0.86), similar to the Ir_xOs_{1-x} alloys described elsewhere [10-11]. $(NH_4)_2[Ir_xRe_{1-x}Cl_6]$ were crystallized by adding an excess

were prepared by thermal decomposition of $(NH_4)_2[Ir_xRe_{1-x}Cl_6]$ in 5-vol.%-H_2/95-vol.%-N_2 stream (15-30 minutes) at 1000 K, followed by natural cooling (10-12 hours).

Hcp-$Ir_{0.71(1)}Re_{0.29(1)}$ and *hcp*-$Ir_{0.23(1)}Re_{0.77(1)}$ were used for high-temperature experiments. *hcp*-$Ir_{0.71(1)}Re_{0.29(1)}$ and *hcp*-$Ir_{0.70(1)}Re_{0.30(1)}$ were characterised in the large-volume press and diamond anvil cell experiments respectively. The *hcp*-$Ir_{0.71(1)}Re_{0.29(1)}$ and *hcp*-$Ir_{0.70(1)}Re_{0.30(1)}$ alloys have nearly identical composition within experimental errors and are cited below as *hcp*-$Ir_{0.70}Re_{0.30}$. Elemental compositions were analysed in 10 points using a Hitachi S-4800 Field Emission scanning-electron microscope (SEM) equipped with energy dispersive X-ray (EDX) analyser (Fig. S1. Table S2).

The thermal decomposition of $(NH_4)_2[Ir_xRe_{1-x}Cl_6]$ (x = 0.23 and 0.70) was investigated *in situ* using the powder X-ray diffraction (PXRD) set-up located at the Swiss-Norwegian Beam Lines (BM01A), ESRF. Samples in powder form were placed in 0.5 mm fused quartz mark tubes (Hilgenberg GmbH, Germany). Tubes were connected to a 2 vol.% H_2/He flow (0.1-0.5 ml/min) and heated with hot air stream from room temperature to 1000 K with a ramp rate of 10 K/min. Temperature was calibrated using the thermal expansion of the cell parameters for silver powder as external standard. The wavelength (λ = 0.68894 Å) and sample-to-detector distance were calibrated using LaB_6 powder (NIST SRM 660c) as external standard. Data were collected every 20 s (approximately every 3 K in the temperature scale) using a PILATUS2M 2D flat detector. The data were converted and diffracted intensities integrated using the SNBL software toolbox [17]. Temperature dependent PXRD patterns were plotted and analysed using the Powder3D software [18]. Parametric

simultaneously for all phases using Rietveld refinement. Selected PXRD profiles upon heating and temperature dependent plots are given in Fig. 2 for $(NH_4)_2[Ir_{0.70}Re_{0.30}Cl_6]$ and in supplementary Fig. S2 for $(NH_4)_2[Ir_{0.23}Re_{0.77}Cl_6]$.

High-pressure PXRD data for *hcp*-$Ir_{0.70}Re_{0.30}$ were collected up to 48 GPa at room temperature at the ID15B beam-line, ESRF, (λ = 0.410962 Å, MAR 555 flat panel detector, beam size 10(*v*)×10(*h*) μm^2). A membrane diamond anvil cell with conically supported Boehler Almax type anvils (300 μm culet sizes) was used for pressure generation. Pressure was determined using a ruby luminescence. Neon was used as pressure-transmitting medium. The diffraction images were recorded under continuous ω-rotation of the DAC from -3 to +3° with 1 second acquisition time. After compression at room temperature, the sample was laser-heated offline up to 2000-2250°C and quenched. The laser-heated sample was investigated at room temperature under pressure (48.5 GPa) and during decompression to ambient pressure.

The large-volume 2000 tons MAVO press in a 6/8(x32) mode with tungsten carbide anvils [20] (ID06-LVP beam-line at the ESRF, λ = 0.2296 Å) was used for experiments with *hcp*-$Ir_{0.70}Re_{0.30}$. A linear pixelated GOS detector was used for *in situ* data collection (sequential exposure of 3.2 seconds at 10 Hz at 32 seconds interval, mounted to intercept the downstream diffraction from the horizontal anvil gap at 1966 mm distance). The detector-beam normal plane was mechanically corrected for tilt and rotation, the detector position was corrected for zero-offset and calibrated against LaB_6 (SRM660a). The *hcp*-$Ir_{0.70}Re_{0.30}$ alloy sample was ground with *h*-BN powder (1:1 volume ratio) in an agate mortar and loaded into a *h*-BN (Goodfellow) capsule, before

equation of state of MgO [23, 24]. The sample was compressed up to 10 GPa and heated up to 3100 K under constant pressure. Compressibility, heating, cooling and decompression curves were collected. Two-dimensional images were integrated to one-dimensional intensities as a function of diffraction angle using the FIT2D software [25]. Unit cell, background, and line-profile parameters were thus refined simultaneously using the model-free full-profile refinement implemented in JANA2006 software [26]. Compressibility curves were fitted using the EoS-Fit 5.2 software [27].

Phase composition and cell parameters of quenched samples recovered from the large-volume press were proved by *in house* powder x-ray diffraction (PXRD) using an ARL X'TRA diffractometer (Cu*K*α-radiation, Ni-filter, Bragg-Brentano reflection geometry, 2Θ = 5-100°, $\Delta 2\Theta$ = 0.03°, 10 s/step, room temperature). A polycrystalline sample was slightly ground with hexane using an agate mortar and the resulting suspension was deposited on the polished side of a quartz sample holder, to form a smooth thin layer after drying. Silicon powder was taken as an external standard (a = 5.4309 Å, FWHM 2Θ = 0.1°) for the calibration.

Cyclic voltammetry (CVA) was performed using an Autolab PGSTAT potentiostat (Eco-Chemie) controlled by a PC with GPES software. Few milligrams of alloys powders were deposited on screen-printed glassy carbon electrodes (GC-SPEs, DropSens C110, S = 0.12 cm^2). 1 M H_2SO_4 water solution was used for background measurements. Electrocatalytic tests were performed in a drop of 1 M Methanol / 1 M H_2SO_4 after 5 minutes conditioning at 0.55 V (*versus* standard hydrogen electrode, SHE). Measured potentials were reported against SHE by using the ferrocyanide |

3. Results.

3.1. Thermal decomposition of $(NH_4)_2[Ir_xRe_{1-x}Cl_6]$ (x = 0.23 and 0.70).

Binary Ir_xRe_{1-x} alloys can be prepared in the whole range of compositions by thermal decomposition of $(NH_4)_2[Ir_xRe_{1-x}Cl_6]$ single-source precursors below 1000 K. Metallic alloys with $x < 0.7$ have *hcp* crystal structure; alloys with $x > 0.85$ are *fcc*-structured. Compositions with $0.7 < x < 0.85$ are two-phase *fcc*+*hcp* mixtures, which corresponds to the equilibrium Ir—Re phase diagram [2].

Recently, the thermal decomposition of $(NH_4)_2[Ir_xOs_{1-x}Cl_6]$ has been linked to the formation of a crystalline intermediate [11]. A similar intermediate phase was detected in the thermal decomposition of the $(NH_4)_2[Ir_{0.70}Re_{0.30}Cl_6]$ salt in the temperature region 550-700 K (Fig. 2). Above 650 K, defect *fcc*- and *hcp*-structured phases form simultaneously. Above 950 K only the *hcp*-$Ir_{0.70}Re_{0.30}$ alloy has been detected. The formation of metallic mixtures with further high-temperature equilibration has been detected in other systems, such as $[Pd(NH_3)_4][PtCl_6]$ and $[Pd(NH_3)_4][IrCl_6]$ [28-29].

Broad diffraction lines characteristic for *hcp*– and *fcc*–structured intermediate metallic phases below 950 K suggest a high concentration of structural defects, such as *fcc/hcp* intergrowths and stacking faults. Since both phases are likely to form intergrowths (rather than separate crystals), it is possible to perform quick thermal annealing and favour phase exchange between the alloys, with the consequent formation of a single phase *hcp*-$Ir_{0.70}Re_{0.30}$ alloy. The simultaneous formation of *fcc*- and *hcp*-structured phases makes this alloy different from the *hcp*-$Ir_{0.50}Os_{0.50}$, in which only one intermediate phase has been detected. The $(NH_4)_2[Ir_{0.23}Re_{0.77}Cl_6]$ salt with lower iridium

3.2. Thermal expansion and compressibility of the *hcp*-$Ir_{0.70}Re_{0.30}$ and *hcp*-$Ir_{0.23}Re_{0.77}$ alloys.

We collected the thermal expansion curves at ambient pressure for two *hcp*-structured alloys, namely *hcp*-$Ir_{0.70}Re_{0.30}$ and *hcp*-$Ir_{0.23}Re_{0.77}$. Neither alloy show any specialities in their thermal expansion curves above 1000 K. Volumetric thermal expansion coefficients in the form $\alpha(T) = \alpha_0 + \alpha_1 T$ were obtained by fitting the temperature dependent atomic volumes to

$$\frac{V(T)}{Z} = \frac{V(T_0)}{Z} exp\left[\int_{T_0}^{T} \alpha(T) dT\right] \quad (3)$$

where $V(T_0)/Z$ is the atomic volume at reference temperature (293 K) (Table 1, Fig. 3).

Hcp-$Ir_{0.70}Re_{0.30}$ and *hcp*-$Ir_{0.23}Re_{0.77}$ alloys have smaller thermal expansion in comparison with pure metals (Fig. 3) and smaller slope in comparison with pure iridium. Pure rhenium has negative thermal dependence of the *c*/*a* ratio, an unusual occurrence in *hcp*-structured metals. However, both *hcp* alloys have positive trend, which is more typical for *hcp*-structured metals such as Os and Ru.

The pressure dependent compressibility curve at room temperature was recorded for *hcp*-$Ir_{0.70}Re_{0.30}$ up to 45 GPa and fitted using the third-order Birch-Murnaghan equation of state (BM-EoS) [10-11, 30-31] (Fig. 3, Table 1). The compressibility curve for *hcp*-$Ir_{0.70}Re_{0.30}$ can be fitted with a relatively large value for the pressure derivate of bulk modulus, which in turn results in lower compressibility of the alloy at high pressures in comparison with pure metals. The *c*/*a* ratio is growing with pressure, making this alloy different from pure Re, those *c*/*a* ratio does not depend on pressure below 100 GPa.

does not result in any phase change and phase separation, which is a proof of the thermodynamic stability of this composition at ambient pressure. High-temperature high-pressure synthesis and phase stability of several Ir─Re alloys were investigated at 1, 4 and 9 GPa up to 2000 K (Table 2, Fig. 1) [12-16]. Several alloys with compositions close to the miscibility gap in Ir─Re phase diagram were used to probe the pressure dependent equilibrium with metallic mixtures and pre-synthetized alloys.

The annealing of Ir/Re mixtures at 2270 K and 4 GPa results in the formation of two-phase samples (Table 2, Fig. 1). This can be associated with a shift of the miscibility gap in the phase diagram upon pressure increase. Re has larger atomic volume, therefore the miscibility gap between *fcc*- and *hcp*-structured alloys shifts towards the rhenium side of the phase diagram. The *hcp*-$Ir_{0.70}Re_{0.30}$ binary alloy is ideal for probing Ir─Re phase relations and equilibrium under high-pressure, since its composition corresponds to the *hcp*-structured alloy with maximal Ir concentration.

Previous experimental data have been obtained *ex situ* using quenched samples prepared in a belt press up to the pressure of 9 GPa [12-16] (Table 2, Fig. 1). In the present study the *hcp*-$Ir_{0.70}Re_{0.30}$ binary alloy was compressed up to 10 GPa in a large-volume press at room temperature and heated with *in situ* diffraction control up to 3000 K. At 10 GPa, *hcp*-$Ir_{0.70}Re_{0.30}$ is stable upon heating up to approximately 2770 K. Above 2770 K, the single-phase alloy decomposes with formation of a two-phase *hcp*+*fcc* mixture. After its formation, the two-phase mixture was annealed for several minutes at 3000 K (at the constant pressure of 10 GPa) and quenched. At 10 GPa, the single-phase *hcp*-structured alloy decomposes to an *fcc*–$Ir_{0.73}Re_{0.27}$ and *hcp*–$Ir_{0.70}Re_{0.30}$

The *hcp*-$Ir_{0.70}Re_{0.30}$ alloy compressed to 45 GPa in diamond anvil cell was laser-heated at 2270-2770 K for 1 minute and quenched to room temperature. The sample recrystallizes into a two-phase mixture (Fig. 4). In eight regions, the cell parameters of *fcc* and *hcp* phases are very similar and vary within experimental errors (Table 2). The shape of the caked diffraction rings suggests high crystallographic strain in the sample after heating under pressure. Phase separation at 48 GPa hints to a slight shift of the miscibility gap with pressure above 10 GPa. The miscibility gap above 10 GPa becomes very narrow.

3.4. Electrocatalytic activity of Ir─Re alloys for methanol oxidation

Several Ir─Re alloys were recently proposed as perspective heterogeneous supported catalysts [5-8]. To preliminarily investigate the catalytic activity of Ir─Re alloys, we tested them to the model reaction of methanol oxidation in acidic aqueous solution.

The recently developed glassy carbon screen-printed electrodes can aid the fast screening of electro-catalytic performances of new metal combinations. The powder can be easily loaded on the horizontal working electrode and analysis can be carried out with few milligrams of powder in a drop of solvent. Nevertheless, due to the presence of a pseudo-reference electrode, potential values should be referred to SHE through the use of an internal redox calibration couple.

Electro-catalytic activity can be estimated from cyclic voltammetry (CV) data from the position of the oxidation peak in the anodic curve. The potential corresponding to the peak maximum in an irreversible electrochemical process is strictly related to its

working electrode has been conditioned at an appropriate potential to achieve adsorption of the molecule on its surface.

Ir and Re do not show pronounced activity in the oxidation of methanol in acidic media. Their oxidation potentials are relatively high: 0.521 V (for Ir) and 0.510 V (for Re). The following activity series can be extracted from the CV curves: two-phase $Ir_{0.85}Re_{0.15}$ (0.470 V) > *hcp*-$Ir_{0.23}Re_{0.77}$ (0.476 V) > *hcp*-$Ir_{0.40}Re_{0.60}$ (0.490 V) > *hcp*-Re (0.510 V) > *fcc*-Ir (0.521 V) ≈ *hcp*-$Ir_{0.70}Re_{0.30}$ (0.521 V) (Fig. 5). The Re-rich Ir─Re alloys show lower potentials in comparison with Ir and Re, which makes them better electrocatalysts for methanol oxidation. The Ir-rich *hcp*-$Ir_{0.70}Re_{0.30}$ alloy has higher peak's potential and therefore lower electrocatalytic activity in comparison with Re.

4. Discussion.

Single-source precursors were proposed as starting materials for active metallic catalysts and porous metals [34]. Recently, several metallic phase diagrams were probed using samples prepared by precursors in mild conditions [35]. Here we report how pressure-dependent phase diagrams can be also probed using pre-specified binary metallic compositions prepared from single-source precursors. Phase separation in *hcp*-$Ir_{0.70}Re_{0.30}$ alloy under high-temperature high-pressure provides information about miscibility gap at high-pressure up to 50 GPa (Fig. 1). Similarly to Ir─Os binary system, the miscibility gap in Ir─Re binary system shifts towards the metal with higher atomic volume (iridium and rhenium respectively) up to 4 GPa. Above 4 GPa, the miscibility gap does not visibly shift and narrows with pressure. The complete *hcp*-$Ir_{0.70}Re_{0.30}$ to *fcc*-$Ir_{0.70}Re_{0.30}$ transformation is not detected below 45-48 GPa. Formation of *hcp*-$Ir_{0.70}Re_{0.30}$ alloy from $(NH_4)_2[Ir_{0.70}Re_{0.30}Cl_6]$

in $(NH_4)_2[Ir_{0.50}Os_{0.50}Cl_6]$, and later the *fcc*-alloy. The *hcp*+*fcc* mixture preformed on early stage of thermal decomposition transforms into the *hcp*-$Ir_{0.70}Re_{0.30}$ alloy above 950 K. The compressibility curve for *hcp*-$Ir_{0.70}Re_{0.30}$ collected at room temperature up to 45 GPa can be fitted with a bulk modulus of 340 GPa, which is smaller in comparison with pure metals. Heating of *hcp*-$Ir_{0.70}Re_{0.30}$ collected at ambient pressure suggests smaller thermal expansion in comparison with Re and Ir. The *c*/*a* ratio for *hcp*-$Ir_{0.70}Re_{0.30}$ is increasing with pressure and temperature, a sensible difference from pure Re, which shows a decrease in the *c*/*a* ratio with temperature and no pressure dependence.

In general, thermal expansion and pressure compressibility of Ir─Re binary alloys follow similar trends as pure Ir and Re metals. At the same time, binary alloys display smaller thermal expansion and pressure compressibility, which can be further exploited to tune the properties of refractory alloys compositions. The miscibility gap in the phase diagram becomes narrower with pressure, a feature which could be exploited in the preparation of single-phase alloys unavailable by direct melting.

We tested the electrocatalytic activity for methanol oxidation of several *hcp*-structured and two-phase (*fcc*+*hcp*) Ir─Re alloys. The best candidate for electro-catalytic oxidation of methanol is thus the two-phase $Ir_{0.85}Re_{0.15}$ alloy. Its high activity can be associated with its high structural defects concentration and with the presence of *fcc*/*hcp* intergrowths. The non-linear dependence of electrocatalytic activity from alloy's composition, a trend showing two minima, should be further investigated for other metallic systems. However, this result suggests that it is necessary to pay attention to

The mechanism of formation of Ir─Re alloys from single-source precursors suggests the presence of a two-phase metallic mixture (*fcc* + *hcp* alloys) in a broad range of temperatures (700-950 K). Such mixture seems to be non-equilibrium and to contain high concentration of structural defects. Considering that the two-phase $Ir_{0.85}Re_{0.15}$ alloy shows higher electrochemical activity, the investigation of non-equilibrium two-phase compositions prepared at temperatures below 900 K may lead to the discovery of new active catalysts with outstanding activity.

5. Conclusions.

In the current study, Ir─Re alloys powders were prepared from single-source precursors under mild conditions and could be potentially used as supported catalysts. In general, oxidation potential increases with Ir concentration and reaches a maximum for the *hcp*-$Ir_{0.70}Re_{0.30}$. Our technique based on single-source precursors can be extended to the preparation of other multicomponent refractory systems, to probe their catalytic and functional properties [36]. Ir─Re alloys prepared from single-source precursors are ideal models to probe the high-pressure high-temperature constitution of binary Ir─Re phase diagram. In the Ir─Re phase diagram, the miscibility gap between *hcp* and *fcc* alloys slightly shifts towards the rhenium side below 4 GPa. Above 4 GPa, the miscibility gap does not drift with pressure and narrows with further compression.

Acknowledgements

The authors thank ID-15B, ID06-LVP and Swiss-Norwegian (BM-01A) beam-lines at the European Synchrotron Radiation Facility (ESRF) for providing us measurement

Financial support by German Science Foundation (DFG), German Ministry of Science and Education (BMBF) and EPSRC Impact Acceleration Account is greatly appreciated.

References:

[1] K.V. Yusenko, Phase Diagram of the Rhenium-Rhodium System: State of the Art, Plat. Met. Rev. 55(3) (2011) 186 doi:10.1595/147106711x579966.

[2] K.V. Yusenko, Phase Diagram of the Iridium-Rhenium System, Plat. Met. Rev. 57(1) (2013) 57 doi:10.1595/147106713x659064.

[3] G. Schneider and A. Boettcher, Deutsche Gold- und Silber-Scheideanstalt, 'Thermocouple', *US Patent* 2,802,894; 1957.

[4] R. D. Lanam, A. R. Robertson and E. D. Zysk, Engelhard Corp, 'Iridium-Rhenium Crucible', *US Patent* 4,444, 728; 1984.

[5] Y. Nakagawa, Y. Shinmi, S. Koso and K. Tomishige, Direct hydrogenolysis of glycerol into 1,3-propanediol over rhenium-modified iridium catalyst, J. Catal., 272(2) (2010) 191 http://dx.doi.org/10.1016/j.jcat.2010.04.009.

[6] Sibao Liu, Yasuyo Okuyama, Masazumi Tamura, Yoshinao Nakagawa, Akio Imaib, Keiichi Tomishige, Selective transformation of hemicellulose (xylan) into n-pentane, pentanols or xylitol over a rhenium-modified iridium catalyst combined with acids, Green Chem. 18 (2016) 165 DOI: 10.1039/c5gc02183a.

[7] Hiroko I. Karan, Kotaro Sasaki, Kurian Kuttiyiel, Carrie A. Farberow, Manos Mavrikakis, Radoslav R. Adzic, Catalytic Activity of Platinum Monolayer on Iridium and Rhenium Alloy Nanoparticles for the Oxygen Reduction Reaction, ACS Catal. 2 (2012) 817 dx.doi.org/10.1021/cs200592x.

catalyst, Reac. Kinet. Mech. Cat. 118 (2016) 481 doi:10.1007/s11144-016-0975-z.

[9] R.H. Tuffias Fabrication Processes for Iridium/Rhenium Combustion Chambers, Mater. Manufact. Process, 13(5) (1998) 773–782 http://dx.doi.org/10.1080/10426919808935298.

[10] K.V. Yusenko, E. Bykova, M. Bykov, S.A. Gromilov, A.V. Kurnosov, C. Prescher, V.B. Prakapenka, M. Hanfland, S. van Smaalen, S. Margadonna, L.S. Dubrovinsky, Compressibility of Ir─Os alloys under high pressure, J. Alloys and Comp., 622 (2015), 155 DOI: 10.1016/j.jallcom.2014.09.210

[11] K.V. Yusenko, E. Bykova, M. Bykov, S.A. Gromilov, A.V. Kurnosov, C. Prescher, V.B. Prakapenka, W.A. Crichton, M. Hanfland, S. Margadonna, L.S. Dubrovinsky, High-pressure high-temperature stability of *hcp*-Ir_xOs_{1-x} (x = 0.50 and 0.55) alloys. J. Alloys and Comp., 700 (2017), 198–207 10.1016/j.jallcom.2016.12.207

[12] A. Panchenko, T. Dyachkova, S. Gromilov, Y. Zaynulin Study of Alloys Ir_xRe_{1-x} (x = 0.65, 0.75 and 0.85) Solid State Phenomena, 203-204 (2013) 55–58 doi:10.4028/www.scientific.net/SSP.203-204.55.

[13] S.A. Gromilov, T.V. Diachkova, E.A. Bykova, N.V. Tarakina, Yu.G. Zainylin, K.V. Yusenko, Thermobaric synthesis of the Ir_xRe_{1-x} ($0.2 < x < 0.4$) solid solutions, Int. J. Mater. Sci. 5 (2013) 476–482 doi: 10.3139/146.110884.

[14] S.A. Gromilov, I.V. Korolkov, K.V. Yusenko, S.V. Korenev, T.V. D'yuchkova, Y.G. Zainulin, A.P. Tutunnik, Phase transformations of the $Re_{0.3}Ir_{0.7}$ solid solution, J. Struct. Chem., 46(3) (2005) 474–478 doi:10.1007/s10947-006-0126-x

7(2) (2012) 93–97.

[16] A. Panchenko, T. Dyachkova, S. Gromilov, Y. Zaynulin Study of Alloys Ir_xRe_{1-x} (x = 0.65, 0.75), XXII Conference on Applied Crystallograhy (Targanice, Poland), Program and Abstracts booklet (2012) 41.

[17] V. Dyadkin, SNBL Tool-box. Grenoble, France: Swiss Norwegian Beamline at ESRF 2013.

[18] P. Rajiv, R. Dinnebier, M. Jansen, Powder 3D Parametric: A program for automated sequential and parametric Rietveld refinement using Topas, Materials Science Forum 651 (2010) 97–104.

[19] TOPAS v.4.0, Bruker-AXS 5465 East Cheryl Parkway – Bruker AXS – 2009.

[20] J. Guignard, W.A. Crichton, The large volume press facility at ID06 beamline of the European synchrotron radiation facility as a High Pressure-High Temperature deformation apparatus. Rev. Sci. Instrum. 86 (2015) 085112. DOI: http://dx.doi.org/10.1063/1.4928151

[21] Y. Le Godec, D. Martinez-Garcia, M. Mezouar, G. Syfosse, J. P. Itie, and J. M.Besson, Thermoelastic behaviour of hexagonal graphite-like boron nitride, High Press. Res. 17 (2000), 35 http://dx.doi.org/10.1080/08957950008200304

[22] A.F. Goncharov, J.C. Crowhurst, J.K. Dewhurst, S. Sharma, Ch. Sanloup, E. Gregoryanz, N. Guignot, and M. Mezouar, Thermal equation of state of cubic boron nitride: Implications for a high-temperature pressure scale, Phys. Rev. B, 75 (2007) 224114. DOI: 10.1103/PhysRevB.75.224114

DOI 10.1007/s002690050070

[24] A. Dewaele, G. Fiquet, D. Andrault▪ , D. Hausermann, P─V─T equation of state of periclase from synchrotron radiation measurements, J. Geophys. Res., 105 (2000), 2869–2877. DOI: 10.1029/1999JB900364

[25] A.P. Hammersley, S.O. Svensson, M. Hanfland, A.N. Fitch, and D. Häusermann, Two-Dimensional Detector Software: From Real Detector to Idealised Image or Two-Theta Scan, High Press. Res., 14 (1996), 235–248. DOI: 10.1080/08957959608201408

[26] V. Petříček, M. Dušek, L. Palatinus Crystallographic Computing System JANA2006: General Features. Z. Krist 229(5) (2014), 345–352 DOI 10.1515/zkri-2014-1737. http://www-xray.fzu.cz/jana/jana.html

[27] R.J. Angel, Equations of State. In Hazen, R.M., Downs, R.T. (Eds.), High-pressure, high-temperature crystal chemistry. Reviews in Mineralogy and Geochemistry, 41 (2001), 35-60. http://www.rossangel.com/

[28] T. Asanova, I. Asanov, A. Zadesenets, E. Filatov, P. Plusnin, E. Gerasimov, S. Korenev, Study on thermal decomposition of double complex salt $[Pd(NH_3)_4][PtCl_6]$. J. Thermal. Anal. Calorim. 123 (2016) 1183–1185. DOI 10.1007/s10973-015-5002-5

[29] T.I. Asanova, I.P. Asanov, Min-Gyu Kim, E.Yu. Gerasimov, A.V. Zadesenets, P.E. Plusnin, S.V. Korenev, On formation mechanism of Pd–Ir bimetallic nanoparticles through thermal decomposition of $[Pd(NH_3)_4][IrCl_6]$. J Nanopart. Res. 15 (2013) 1994–2009. DOI 10.1007/s11051-013-1994-6

Russian), 2(5) (1977), 1026–1029.

[31] J.W. Arblaster, Crystallographic Properties of Iridium Assessment of properties from absolute zero to the melting point, Platinum Met. Rev., 54 (2010), 93–102. DOI: 10.1595/147106710X493124

[32] Y. Cerenius, L. Dubrovinsky, Compressibility measurements on iridium, J. Alloys Compd, 306(1-2) (2000), 26–29. DOI: 10.1016/S0925-8388(00)00767-2

[33] L. Dubrovinsky, N. Dubrovinskaia, V.B. Prakapenka, A.M. Abakumov, Implementation of micro-ball nanodiamond anvils for high-pressure studies above 6 Mbar, Nat. Commun. 3(1163) (2012), 1–7. DOI: 10.1038/ncomms2160.

[34] M. Avisar-Levy, O. Levy, O. Ascarelli, I. Popov, A. Bino, Fractal structures of highly-porous metals and alloys at the nanoscale, J. Alloys Comp. 635(25) (2015) 48–54 http://dx.doi.org/10.1016/j.jallcom.2015.02.073.

[35] Y.V. Shubin, P.E. Plusnin, S.V. Korenev, Determination of the equilibrium miscibility gap in the Pd–Rh alloy system using metal nanopowders obtained by decomposition of coordination compounds, J. Alloys Comp. 622 (2015) 1055–1060 http://dx.doi.org/10.1016/j.jallcom.2014.10.187

[36] KV Yusenko, S Riva, PA Carvalho, MV Yusenko, S Arnaboldi, A Sukhikh, M Hanfland, SA Gromilov. First hexagonal close packed high-entropy alloy with outstanding stability under extreme conditions and high electrocatalytic activity in methanol oxidation, Scripta Materialia, 138 (2017), 22–27 https://doi.org/10.1016/j.scriptamat.2017.05.022

and *hcp* (*hexagons*) alloys; firm lines represent polynomial individual fittings for *fcc*- and *hcp*-structured alloys individually according to Equations 1 and 2). Phase diagram was calculated in [2] using regular solutions model. *Right*: Phase separation for 0.80Ir+0.20Re and 0.75Ir+0.25Re mixtures [12-16] and in *hcp*-$Ir_{0.70}Re_{0.30}$ after annealing above 2000 K under compression (*circles* represent two-phase compositions).

Fig. 2. *Left*: Selected PXRD patterns obtained at various temperatures corresponded to the thermal decomposition of $(NH_4)_2[Ir_{0.70}Re_{0.30}Cl_6]$ (2 vol.% H_2/He flow, λ = 0.68894 Å). *Right*: weight fractions for intermediate phases upon heating (inset corresponds to the 2D-film top view of the temperature dependent PXRD patterns upon heating).

Fig. 3. *Left*: thermal expansion of *hcp*-$Ir_{0.23}Re_{0.77}$ and *hcp*-$Ir_{0.70}Re_{0.30}$ alloys on heating (red hexagons) and cooling (blue hexagons). Line corresponds fitting with Equation 3. *Middle*: thermal dependence of *c*/*a* ratio for *hcp*-$Ir_{0.23}Re_{0.77}$ and *hcp*-$Ir_{0.70}Re_{0.30}$ alloys and Re [30] (lines correspond to 2^{nd} order polynomial fits). *Right*: Pressure dependence of atomic volume for *hcp*-$Ir_{0.70}Re_{0.30}$, pure Ir [31] and Re [30] (lines show the third-order BM-EoS fits). Inset shows pressure dependence of *c*/*a* ratio.

Fig. 4. A: *In situ* PXRD data collected at the large-volume press for *hcp*-$Ir_{0.70}Re_{0.30}$ at constant pressure (10 GPa) with increasing temperature between 2000 and 3000°C (2D-film top view, ESRF ID06-LVP, λ = 0.2296 Å) and selected PXRD patterns collected at 2000 and 3000 K. PXRD data collected before (B: 45 GPa, room temperature) and after (C: 48.3 GPa, room temperature) laser heating at 2000-2500 °C of the *hcp*-$Ir_{0.70}Re_{0.30}$ alloy (ESRF ID15B, λ = 0.410962 Å).

on glassy-carbon screen-printed electrodes. *Blue line* – first cycle after absorption; *grey line* – second cycle after absorption (background). Current is normalized for the working electrode surface area. Potentials are reported against SHE by using the ferrocyanide | ferricyanide redox couple as internal standard.

Table 1. Volumetric thermal expansion parameters at ambient pressure and bulk moduli at room temperature for pure Ir, Re and *hcp*-structured Ir–Re alloys.

Composition	V_0/Z, Å$^3\cdot$atom^{-1} [a]	V_0/Z, Å$^3\cdot$atom^{-1} [b]	$\alpha_0\cdot10^5$, K^{-1}	$\alpha_1\cdot10^9$, K^{-2}	$\alpha_{293}\cdot10^5$, K^{-1}	B_0, GPa / B_0` [c]	Refs.
hcp-Re (ambient pressure)	14.720(1)	14.73(1)	1.6(1)	-0.04(1)	1.601	353(3) / 4	[30, 33]
hcp-$Ir_{0.23(1)}Re_{0.77(1)}$	14.502(1)[d]	–	1.12(4)	5.7(3)	1.287	–	present study
hcp-$Ir_{0.71(1)}Re_{0.29(1)}$	14.184(2)[e]	–	1.32(6)	5.2(4)	1.472	–	present study
hcp-$Ir_{0.70(1)}Re_{0.30(1)}$	14.184(1)[f]	14.184(2)	–	–	–	340(3) / 7.6(2)	present study
fcc-Ir	14.1475(3)	–	1.66(2)	7.3(3)	1.874	354(6) / 5.80(7)	[31, 32]

[a]atomic volume refined from PXRD data at ambient conditions (in house data);

[b]atomic volume refined from BM-EoS;

[c]B_0 – bulk modulus, B_0` – pressure derivative of bulk modulus;

[d]*hcp*-$Ir_{0.23(1)}Re_{0.77(1)}$: a = 2.759(1), c = 4.400(2) Å;

[e]*hcp*-$Ir_{0.71(1)}Re_{0.29(1)}$: a = 2.735(2), c = 4.380(4) Å;

[f]*hcp*-$Ir_{0.696(5)}Re_{0.304(5)}$: *a* = 2.737(1), *c* = 4.372(2) Å.

hcp–$Ir_{0.70}Re_{0.30}$	Ambient pressure 800°C, 1 h	*hcp*–$Ir_{0.70}Re_{0.30}$	2.736(2) 4.390(3)	14.23(1)	[14]
hcp–$Ir_{0.70}Re_{0.30}$	1 GPa, 1900°C, 5 min	*fcc*–$Ir_{0.70}Re_{0.30}$	3.846(2)	14.22(1)	[14]
0.85Ir+0.15Re	4 GPa, 2000°C, 10 min	*fcc*–$Ir_{0.85}Re_{0.15}$	3.8470(4)	14.233	[15]
0.80Ir+0.20Re	4 GPa, 2000°C, 5 min	*fcc*–$Ir_{0.80}Re_{0.20}$	3.845(2)	14.21(2)	[13]
0.75Ir+0.25Re	4 GPa, 2000°C, 10 min	*90 wt.% fcc*–$Ir_{0.76}Re_{0.24}$	3.844(3)	14.21(2)	[12, 16]
		10 wt. % hcp-$Ir_{0.68}Re_{0.32}$	2.744(2) 4.364(4)	14.23	
0.75Ir+0.25Re	4 GPa, 2000°C, 15 min	68 wt.% *fcc*–$Ir_{0.87}Re_{0.13}$	3.842(2)	14.18(2)	[13]
		32 wt.% *hcp*–$Ir_{0.65}Re_{0.35}$	2.741(1) 4.377(2)	14.24(4)	
0.65Ir+0.35Re	4 GPa, 2000°C, 10 min	*6 wt.% fcc*–$Ir_{0.77}Re_{0.23}$	3.844(3)	14.21(2)	[12, 16]
		94 wt. % hcp-$Ir_{0.70}Re_{0.30}$	2.742(2) 4.368(4)	14.22	
0.60Ir+0.40Re	4 GPa, 2000°C, 5 min	*fcc*–$Ir_{0.60}Re_{0.40}$	2.725(1) 4.371(2)	14.33(4)	[13]
hcp–$Ir_{0.70}Re_{0.30}$	9 GPa, 1900°C, 10 min	80 wt.% *fcc*–$Ir_{0.75}Re_{0.25}$	3.848(2)	14.245(5)	[14]
		20 wt.% *hcp*–$Ir_{0.65}Re_{0.35}$	2.742(2) 4.374(3)	14.241(5)	
hcp–$Ir_{0.70}Re_{0.30}$	10 GPa, 3000°C, 10 min	47 wt.% *fcc*–$Ir_{0.73}Re_{0.27}$	3.849(3)	14.255(5)	present study
		53 wt.% *hcp*–$Ir_{0.70}Re_{0.30}$	2.739(2) 4.375(3)	14.212(5)	
hcp–$Ir_{0.70}Re_{0.30}$	48.3 GPa, 2000-2500°C, 1 min	*fcc*–$Ir_{0.74}Re_{0.26}$	3.848(1)	14.250(2)	present study
		hcp–$Ir_{0.65}Re_{0.35}$	2.742(2) 4.376(3)	14.244(1)	

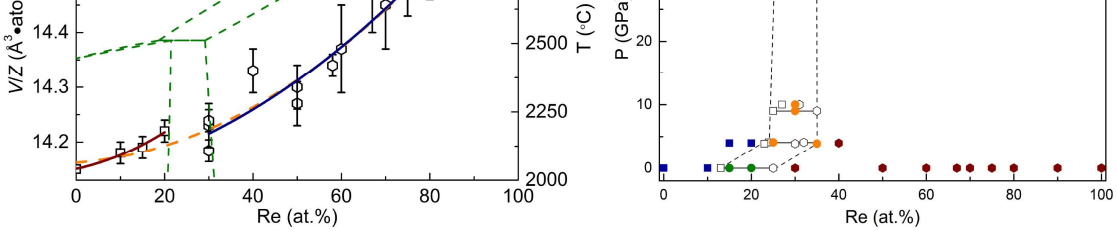

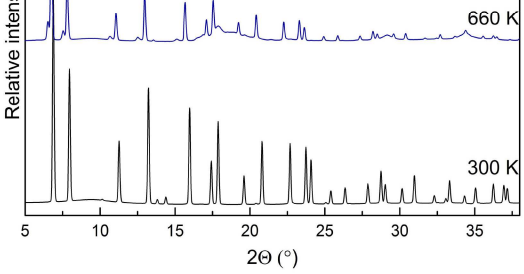

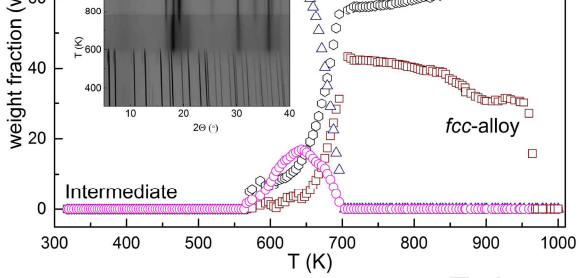

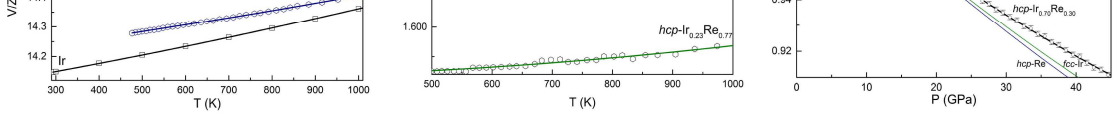

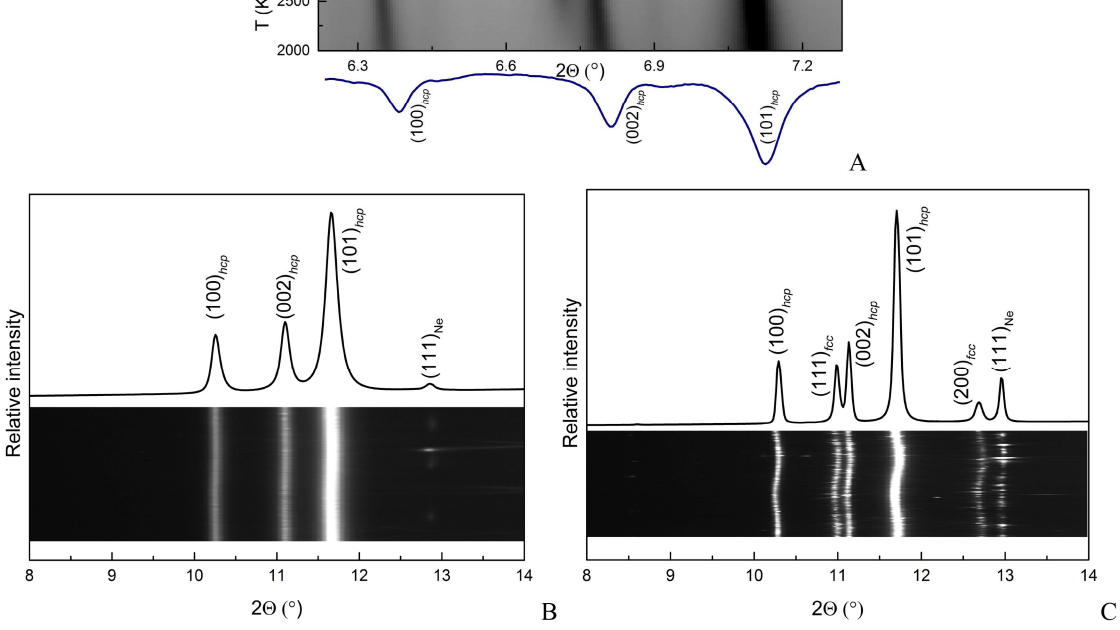
T (K)
2500
2000
6.3
6.6
6.9
7.2
2Θ (°)
(100)hcp
(002)hcp
(101)hcp
A
Relative intensity
(100)hcp
(002)hcp
(101)hcp
(111)Ne
8
9
10
11
12
13
14
2Θ (°)
B
Relative intensity
(100)hcp
(111)fcc
(002)hcp
(101)hcp
(200)fcc
(111)Ne
2Θ (°)
C